Oxygen lone-pair states near the valence band edge of aluminum oxide thin films

Z. W. Zhao, B. K. Tay,[a] Chang Q. Sun, and V. Ligatchev
School of Electrical and Electronic Engineering, Nanyang Technological University, Singapore, 639798

(Received 9 July 2003; accepted 25 January)

Deep level transient spectroscopy and optical absorption spectroscopy measurement revealed three outstanding features of density-of-states (DOS) appeared above the valence band edge (E_v) of Al oxide thin films. The broad peak located at 0.39 eV above E_v disappears while the other two located at 1.0 and 1.3 eV shift in position and attenuate in intensity upon annealing at 200 °C. The latter two peaks are removed by annealing at temperature up to 400 °C. The observed midgap DOS feature dynamics is in accordance with the oxygen lone pair features as confirmed earlier with Raman spectroscopy in the low-frequency ranges [C. Q. Sun *et al.*, J. Appl. Phys. **90**, 2615 (2001)] and thermal desorption measurements of other oxide surfaces. © *2004 American Institute of Physics.* [DOI: 10.1063/1.1686905]

I. INTRODUCTION

Catalytic oxidation is common to most branches of natural science and engineering: from fields such as environmental chemistry (CO oxidation and ozone protection) and biological chemistry (DNA folding and protein signaling) to pharmaceutical chemistry (NO regulator and messenger).[1–3] Oxidation of metal thin films relates to the foundation of applications in microelectronics (metal-oxide-semiconductor field effect transistor gate device and sensors), photoelectronics (luminescence, conductance and filed emission), magnetoelectronics (giant magnetoresistance and superconductivity), etc.[4,5] Therefore, a comprehensive understanding of the electronic structure upon bond formation in terms of density-of-states (DOS) has attracted much attention. A recent chemical-bond, valence band, and surface potential barrier correlation theory has been intensively and systematically verified,[1] which indicates that four essential DOS features are produced and added to the valence band or above of the host upon oxidation, i.e., the bonding, nonbonding lone pair, holes and antibonding dipoles, which dominate the performance of an oxide compound. In the present work, we report observations that confirm the presence of the predicted DOS features of holes and nonbonding lone pair DOS near the valence band edge (E_v) of aluminum oxide thin film. The DOS features were derived from deep level transient spectroscopy (DLTS) and optical absorption spectroscopy probing the Al oxide thin films annealed at temperatures in the range of 200–600 °C.

II. EXPERIMENT

The as-grown films were obtained by using off-plane filtered cathodic vacuum arc (FCVA) technique at room temperature. The FCVA system incorporates an off-plane double-bend filter to effectively remove macroparticles.[6,7] An Al cathode with a purity of 99.98% operated at an arc current of 120 A was used to obtain the plasma. The base pressure of the system was 4×10^{-6} Torr. The reactive gas of oxygen was introduced into the plasma stream within the filter region of the FCVA system. The films with thickness around 600 nm were grown on *n*-type Si (100) and quartz substrates at room temperature with the process pressure of 5×10^{-4} Torr. The films grown on quartz substrates were then annealed in a quartz tube furnace at 200, 400, and 600 °C for 400 min in air and then cooled in a furnace in air to room temperature.

For DLTS test, a pure Al layer with thickness of 0.1–0.2 μm was deposited on the top of the aluminum oxide thin film by sputtering onto Si substrate to form metal-oxide-semiconductor structure. Both dc current–voltage ($I-V$) characteristics and the relation between reciprocal square structure capacitance (C^{-2}) and inverse voltage (V) have to be measured in order to prove the applicability of the DLTS technique to the film characterization. Rectifying $I-V$ characteristics and linear relation between C^{-2} and V will allow DLTS to be carried out. Using ''Bio Rad'' DL 8000 system, DLTS was carried out on the structure of ''Al/AlO_x/*n*-Si'' sandwich at 1 MHz frequency of capacitance measurements in ''double boxcar'' mode under the vacuum condition with gradually increased temperature. A 10 V reverse bias and a 5 V of ''negative'' voltage pulse with 100 μs pulse duration were applied to the structure of Al/AlO_x/*n*-Si in the ''electrical pulse'' regime. The temperature-dependent capacitance difference, $\Delta C(T)$, was obtained between the time at $t_1=360$ μs and the time $t_2=20.48$ ms. The original DLTS data were then recorded in the temperature range of 20–315 K. The contact area of pure Al layer on top of film was estimated to be 5×10^{-2} cm^2. The film thickness was measured by using a Tencor P-10 Surface Profiler. Transmittance and reflectance of the films were recorded by using a Perkin-Elmer Lamda 16 UV/VIS spectrometer from 200 to 900 nm. Absorption coefficient of the films was obtained by fitting optical spectra using Scout software.[8]

[a]Author to whom correspondence should be addressed; electronic mail: ebktay@ntu.edu.sg

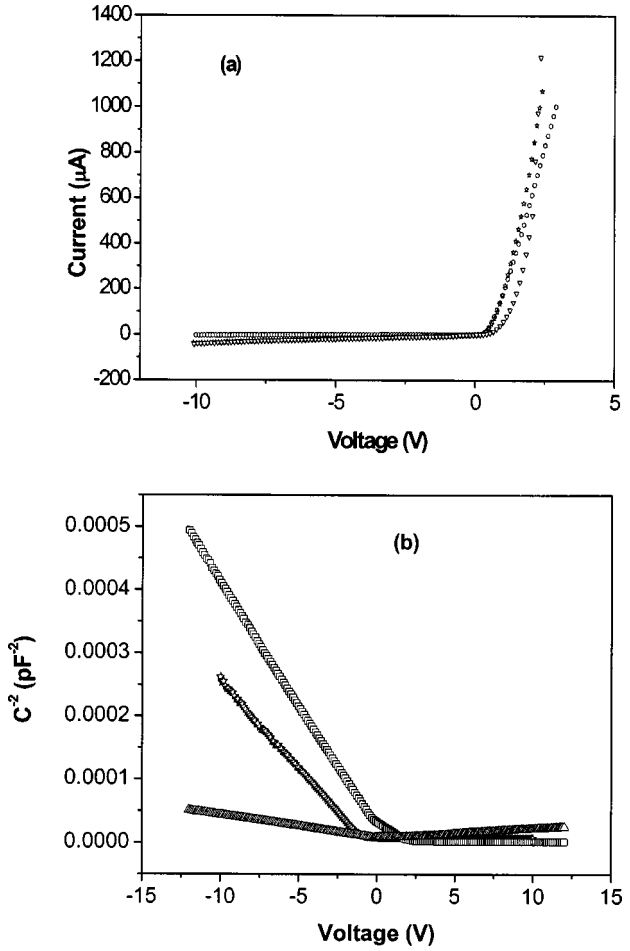

FIG. 1. The dc $I-V$ characteristics (a) and $C^{-2}-V$ characteristics (b) of the $Al/AlO_x/n$-Si structure.

III. RESULTS AND DISCUSSION

A. DOS features of Al oxide films from DLTS results

Figure 1(a) shows the typical curves of $I-V$ characteristics of $Al/AlO_x/n$-Si structure measured using the DLTS equipment. The rectifying behavior is observed from the $I-V$ curves, which suggests the p-type dc conductivity in the AlO_x films. The results from the typical curves of $C^{-2}-V$ reveal the near linear relationship in the reverse voltage range as shown in Fig. 1(b). These experiments confirm the existence of the depletion area at the AlO_x/n-Si interface.

For the as-grown film, the DOS distribution, $N(E)$, could be deconvolved from the original DLTS data according to special ''regularization'' algorithm given in Ref. 9. As shown in Fig. 2, near the E_v, the $N(E)$ tail states exponentially decay into the forbidden gap, which are caused by the departure of the bond length and bond angles arising from the structure long range disorder of the film. The exponential tail can be expressed as[10]

$$N(E)=N_0\exp(-E/kT_v), \tag{1}$$

where E is the energy away from the valence band edge, E_v; k is the Boltzmann constant. The characteristic temperature

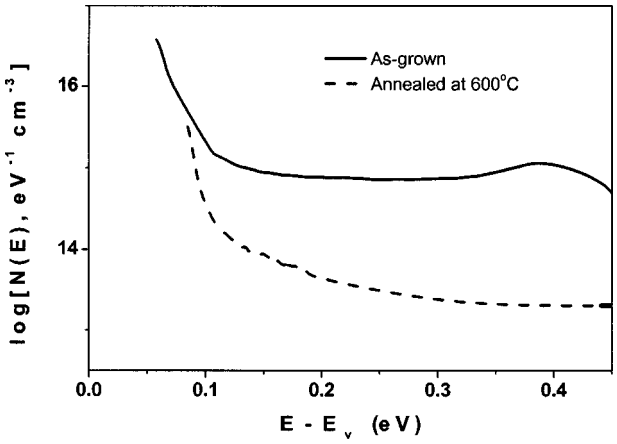

FIG. 2. DOS distribution in as-grown film and annealed film at 600 °C as derived from DLTS.

T_v is used to describe the slope of the band tail. From the distribution of $N(E)$, the derived slope of exponent is around 45 meV corresponding to $T_v \sim 520$ K.

Besides, a $N(E)$ peak density with 1.5×10^{15} cm^{-3} eV^{-1} presents at 0.39 eV away from the E_v. The full width at half maximum of the peak is ~54 meV, showing the characteristics of amorphous phase of the film. This feature near the E_v arises from the coordination number defects,[10] which may be caused by oxygen vacancies in the film giving rise to emergence of hole traps near the valence band edge. It is worth noting that this feature disappears in $N(E)$ distribution of the film annealed at 600 °C as shown in Fig. 2.

B. Absorption coefficient and the DOS features

Figure 3 shows the dispersion curves of absorption coefficient for the films. For the as-grown film, as can be seen, the variation of absorption coefficient is strongly dependent on the incident photon energy. In the range of photon energy less than 4 eV, no significant features can be resolved in the spectra. Beyond this range, an increase in the absorption coefficient can be observed, which suggests that the incident photon energy approaches the band gap value. A broad peak

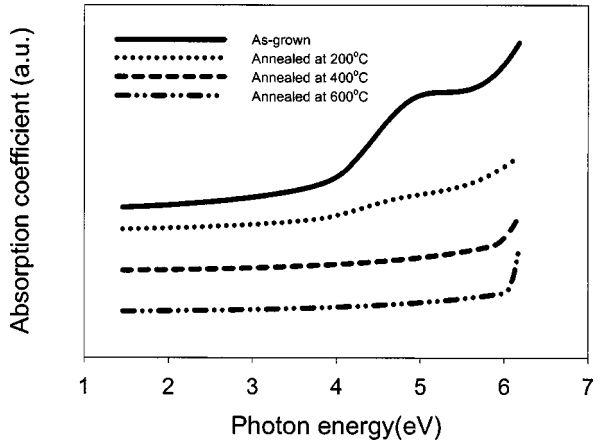

FIG. 3. Dispersion curves of absorption coefficient of the as-grown and annealed films.

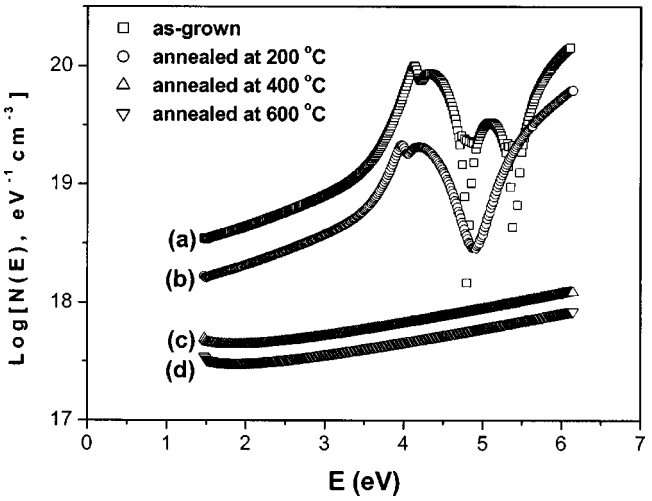

FIG. 4. DOS spectra, deconvoluted from the absorption coefficient in Fig. 3 using regularization algorithm (see Ref. 12).

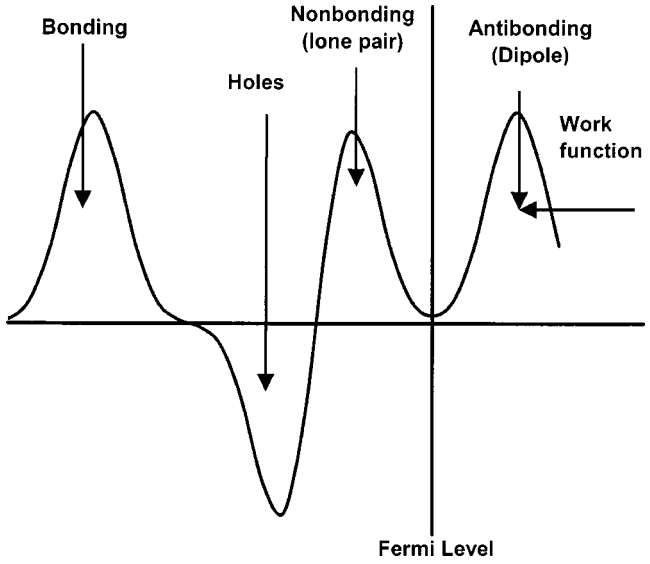

FIG. 5. Illustration of oxygen derived DOS features of bonding, holes, nonbonding lone pair and the antibonding dipoles (see Refs. 14–17). Hole production creates the band gap and turns the Al oxide into an insulator or semiconductor; the lone-pair feature is within the band gap but its position varies from material to material.

is observed centered around 4.9 eV, which is related to the defects existing in the film. In addition, the Urbach edge is clearly observed near the photon energy of 6 eV, which is the typical characteristic of amorphous materials. For such a sample, the optical absorption has an exponential energy dependence, which can be expressed as[10]

$$\alpha(h\upsilon) = \alpha_0 \exp[(h\upsilon - E_g)/E_0], \tag{2}$$

where α is the absorption coefficient, $h\upsilon$ the photon energy, E_0 the Urbach tail slope and E_g the band gap of the material. The E_0 is estimated around 0.94 eV.

It is found that the absorption coefficient for the annealed films depends strongly on the annealing temperature, especially in the range of higher photon energy. Note that the broad absorption peak in the as-grown film disappears upon annealing at temperature above 200 °C, which is consistent with the $N(E)$ distribution of the annealed film as shown in Fig. 2. The Urbach edge becomes sharper and less intense with increasing annealing temperature, which indicates the essential reduction in concentration of the defects states (e.g., oxygen vacancies, coordination defects) in the band tail.

For the as-grown film, the optical band gap, E_g, determined from the Tauc plot,[11] is estimated to be 5.4 eV. The broad peak is centered at 5 eV in the absorption coefficient curve and has a deviation of 0.4 eV from E_g. This value is in good agreement with previous DLTS results discussed in Fig. 2, where a peak is located 0.39 eV away from the E_v. The $N(E)$ can be deconvoluted from the absorption data using a regularization algorithm.[12] Figure 4 shows the annealing temperature dependence of the $N(E)$ distribution. In general, the occupied DOS in the as-grown film is much higher compared with others. As the annealing temperature increases, the $N(E)$ decreases rapidly, especially at temperatures higher than 200 °C.

Besides the peak at 0.4 eV that matches the DLTS results, two additional $N(E)$ peaks in the forbidden gap are identified to locate at 4.4 and 4.1 eV, in Fig. 4, which correspond to $\Delta E_1 = 1.0$ eV and $\Delta E_2 = 1.3$ eV above the E_v, respectively. DLTS and absorption measurement detect only one peak because its range limit is up to 0.85 eV away from the E_v.[13] These two peaks ($\Delta E_1 = 1.0$ eV; $\Delta E_2 = 1.3$ eV) are beyond the scope of DLTS. The peak in curve (a) at $\Delta E = 0.4$ eV turns out to be flat when the sample is annealed at 200 °C as shown in curve (b), which also agrees with the results shown in Fig. 3. The higher energy peaks in curve (a) shift to lower photon energy as compared in curve (b), which might be caused by the shrinkage of the band gap after annealing.[10] All the peaks disappear upon further increasing the annealing temperature to 400 °C, as shown in curves (c) and (d).

C. Mechanism

DOS distribution below the Fermi level of metal oxide can be obtained by density functional theory calculations and experimental observations. Tight-binding theory calculations revealed four DOS features of O–Ru $(10\bar{1}0)$ surfaces[14] coinciding with photoelectronic spectroscopy profiles from O–Pd (110)[15] and O–Cu (110)[16] surfaces, and the bond-band-barrier correlation description[1,17] Figure 5 illustrates the oxygen derived DOS features. It is essential for an oxygen atom to hybridize its *sp* orbital upon interaction with solid atoms. Bonding, nonbonding lone pairs, holes and antibonding dipoles are involved in the reaction, which add corresponding DOS features to the host. As such, the current observed midgap DOS features of aluminum oxide thin films in Fig. 4 could easily be understood in terms of the oxygen lone pairs and amorphous structures. The peak located at 5 eV in Fig. 4(a), which disappears easily at 200 °C in Fig. 4(b), can be attributed to defect states due to the coordination imperfection in amorphous states. Another two peaks are originated from nonbonding lone pairs and both have a shift in position and decrease in intensity when the film is annealed at 200 °C. At the critical temperature of 400 °C, the

lone pair feature disappears corresponding to the broken of nonbonding lone pair, or reduction of the oxidation, which agrees well with the low-activation thermal desorption features of O–Pd (110) (387 °C)[15] and O–Rh (111) (427 °C)[18] surfaces. The lone pair features in the O–Cu (001) surface also disappear after annealing at 400 °C as confirmed with very-low-energy electron diffraction.[19] The existence of the lone pair in Al and Ti oxides has been confirmed using Raman spectroscopy.[1] Using Raman spectroscopy, two peaks have been observed below 1000 cm^{-1} in Al oxide. As the stronger part of a hydrogen bond, the covalent-bond vibration contributes to the spectrum at much higher frequencies. Thus, these low-frequency features below 1000 cm^{-1} observed in Raman spectrum in Al oxide come from the vibration of the lone-pair induced dipoles, being similar to those observed from biomolecules[20] and it is evident for the existence of lone pairs in Al oxide.

Ruchschloss *et al.*[21] and Schneider *et al.*[22,23] suggested that hydrogen is involved during the deposition of alumina and other oxide thin films. The metal (silicon) oxide hydroxide formation, or the presence of OH, is suggested to be responsible for the blueshift in the photoluminescence of Si and metal oxide films. Here we refer the midgap states to the lone pair state that is intrinsic of oxygen or nitrogen upon *sp*-orbital hybridization. The presence of the lone-pair features in an oxide, or a nitride,[24] is independent of the bonding partner, whether a metal, silicon, carbon or even hydrogen. Therefore, the lone-pair DOS features do not reflect the existence of minor impurities in the films.

IV. CONCLUSIONS

Three outstanding midgap DOS features of Al oxide have been identified with DLTS and optical absorption spectroscopies. The DOS feature at 0.39 eV, which disappears at 200 °C, is ascribed as the amorphous band tail states. The two midgap lone-pair states at 1.0 and 1.3 eV disappear at 400 °C, which coincides not only with the thermal desorption features but also x-ray photoelectron spectroscopic DOS features from other metal-oxide surfaces, which are within the bond-band-barrier correlation prediction for oxide formation. Practice may provide an effective way for closer examination of the electronic behavior in an oxide compound.

[1] C. Q. Sun, B. K. Tay, S. P. Lau, X. W. Sun, X. T. Zeng, H. Bai, H. Liu, Z. H. Liu, and E. Y. Jiang, J. Appl. Phys. **90**, 2615 (2001).
[2] C. Q. Sun, Prog. Mater. Sci. **48**, 521 (2003).
[3] C. Q. Sun and S. Li, Surf. Rev. Lett. **7**, 213 (2000).
[4] J. F. Moore, D. R. Strongin, P. B. Comita, M. W. Ruckman, and M. Strongin, Appl. Phys. Lett. **65**, 368 (1994).
[5] C. Jeong, B. Lee, and S. Joo, Mater. Sci. Rep. **16**, 59 (2001).
[6] X. Shi, B. K. Tay, H. S. Tan, L. Zhong, Y. Q. Tu, and S. R. P. Silva, J. Appl. Phys. **79**, 7234 (1996).
[7] X. Shi, B. K. Tay, and S. P. Lau, Int. J. Mod. Phys. B **14**, 136 (2000).
[8] W. Theiss, in *Scout Thin Film Analysis Software Handbook*, edited by M. Theiss (Hard-and Software, Aachen, Germany).
[9] V. Ligatchev, S. F. Yoon, J. Ahn, Q. Zhang, and Rusli, Radiat. Eff. Defects Solids **154**, 261 (2001).
[10] R. A. Street, *Hydrogenated Amorphous Silicon* (Cambridge University Press, Cambridge, 1991).
[11] K. Seeger, *Semiconductor Physics*, Springer Series in Solid-State Science, Vol. 40, 3rd ed. (Springer, Berlin, 1985).
[12] V. A. Ligatchev and V. A. Filikov, Sov. Phys. Semicond. **25**, 78 (1991).
[13] V. Ligatchev, S. F. Yoon, J. Ahn, Q. Zhang, Rusli, S. Zhgoon, and K. Chew, Diamond Relat. Mater. **10**, 1335 (2001).
[14] S. Schwegmann, A. P. Seitsonen, V. De Renzi, H. Dietrich, H. Bludau, M. Gierer, H. Over, K. Jacobi, M. Scheffler, and G. Ertl, Phys. Rev. B **57**, 15487 (1998).
[15] V. A. Bondzie, P. Kleban, and D. J. Dwyer, Surf. Sci. **347**, 319 (1996).
[16] S. Hufner, *Photoelectron Spectroscopy: Principles and Applications* (Springer, Berlin, 1995), p. 339.
[17] C. Q. Sun, Appl. Phys. Lett. **72**, 1706 (1998).
[18] A. D. Logan, A. K. Datye, and J. E. Houston, Surf. Sci. **245**, 280 (1991).
[19] C. Q. Sun, Surf. Rev. Lett. **8**, 367 (2001); **8**, 703 (2001).
[20] W. G. Han and C. T. Zhang, J. Phys.: Condens Matter **3**, 27 (1991).
[21] M. Ruchschloss, Th. Wirschem, H. Tamura, G. Ruhl, J. Owald, and S. Veprek, J. Lumin. **63**, 279 (1995).
[22] J. M. Schneider, A. Anders, B. Hjorvarsson, I. Petrov, K. Macak, U. Helmersson, and J. E. Sundgren, Appl. Phys. Lett. **74**, 200 (1999).
[23] J. M. Schneider, A. Anders, and G. Y. Yushkov, Appl. Phys. Lett. **78**, 150 (2001).
[24] W. T. Zheng, J. J. Li, X. Wang, X. T. Li, Z. S. Jin, B. K. Tay, and C. Q. Sun, J. Appl. Phys. **94**, 2741 (2003).